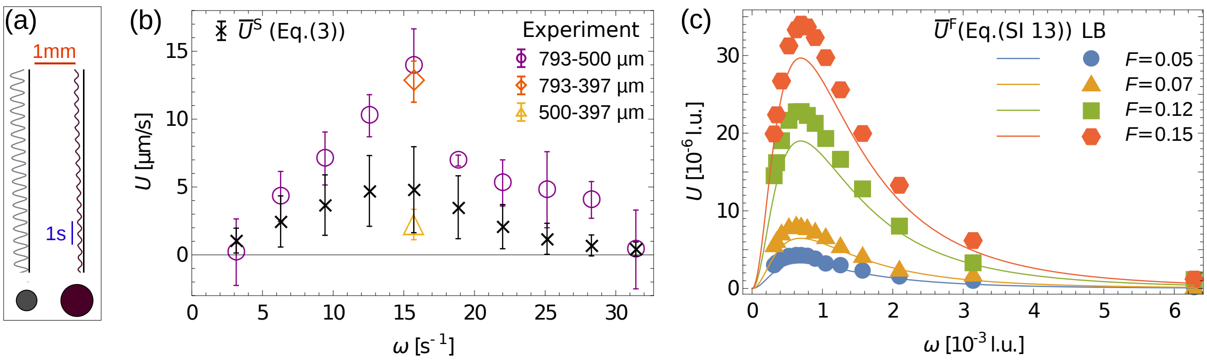

FIG. 2. **Swimming dynamics of an asymmetric dumbbell - comparison of LB simulations and experiments with the analytic model** (a) Sinusoidal trajectory of the beads (500 and 800μm) subject to the driving $B_z = 5.6\,\mathrm{mT}$, $B_0 = 0.7\,\mathrm{mT}$, $b = 0.35\,\mathrm{mT}$ and $\omega = 12.57\,\mathrm{Hz}$. Vertical lines are guides to the eye. (b) Average swimming speed of the asymmetric dumbbell as a function of the magnetic field frequency ω. Amplitudes of the field are as in (a). Error bars account for the variance ($\pm\sigma$) between 5 independent experiments. Theory using Eq.(3) is shown in black for the $500 - 793\mu$m beads combination, with the error bars propagated from experimental uncertainty. (c) Average swimming speed of the asymmetric dumbbell as a function of the frequency from lattice Boltzmann simulations (symbols) and the analytic model (lines) for different values of the driving force F (no fitting). Parameters are same as in Fig. 1 except that $k = 1/200$.

numbers were obtained in previous experiments involving the linear 3-bead swimmer [27].

In order to understand the role of the swimmer inertia, we analyze the frequency response of the swimming speed of the dumbbell (Fig. 2b,c) using all three approaches, whereby the parameters of the simulations are adjusted to recover the experimental swimmer geometry. In experiments, the investigated frequency range corresponds approximately to $\mathrm{Re_s} \sim 1.5$ up to $\mathrm{Re_s} \sim 15$, with the radius of the small bead used as the characteristic length (Fig. 2b). This is matched in simulations where $\mathrm{Re_s}$ ranges from 0.38 to 7.54 for the frequencies considered (Fig. 2c), while $\mathrm{Re_f}$ remains small at $\mathrm{Re_f} < 2\times10^{-3}$.

For low frequencies corresponding to $\mathrm{Re_s} \ll 1$, with $\mathrm{Re_f} \ll 1$, the asymmetric swimmer obeys the usually-encountered Stokesian *scallop theorem* for microswimmers [1]. Consequently, the dumbbell swims inefficiently. A vanishing swimming speed is also observed at high frequencies in all approaches as the amplitude of oscillation decreases too. The intermediate frequencies are characterized by a broad peak in the dumbbell speed. Following the analytic model, this maximum should be associated with the mechanical resonance of the dumbbell. Specifically, Eq. (2) possesses an optimal swimming frequency close to ω_0, a signature of the influence of the swimmer inertia. This maximum is thus by nature different to the optimum frequency occurring for purely Stokesian dynamics [6, 31]. In experiments the maximum appears at a frequency of around $15\,\mathrm{s}^{-1}$, which corresponds to the characteristic mechanical resonance identified previously [25, 27]. In simulations, it occurs around $\mathrm{Re_s} = 1.5$, which corresponds well to $\omega_0 \sim 1.22 \times 10^{-3}\,\mathrm{l.u.}$.

Finally, we compare the analytic model directly with the experiments (Fig. 2b) and simulations (Fig. 2c). Rather than using Eq.(2), we use SI-Eq.(13) (no restriction on a_i/L), due to the proximity of the beads in the simulations. With no fitting parameters, the agreement is excellent, with the error not exceeding 10%. The strongest deviations are found around the peak velocity, where the non-zero fluid inertia may play a small role [18, 20, 21]. Furthermore, from reading out the stroke amplitude obtained in experiments, the measured velocities can be compared to the model using Eq. (3). Once again, a very good agreement is obtained with some differences in speed amplitudes at higher frequencies. This deviation is attributed to the presence of the interface and the non-linearity of the magneto-capillary potential, which are not captured by the model.

Those comparisons not only vindicate the theoretical model but also testify towards the existence of a mesoscopic swimming regime where propulsion is driven by the inertia of the device while keeping a low $\mathrm{Re_f}$. Self-propulsion of mesoswimmers relies on $\mathrm{Re_s} > 1$, which points to the significant role of the inertia of the beads. However, as demonstrated by the behavior of the symmetric design, inertia alone is not able to propel with a reciprocal deformation. Indeed, swimming necessitates the asymmetry of the design. Under the application of forces, beads accelerate and decelerate at a different rate as soon as $\theta_i \neq 0$ [24]. A direct consequence of this asymmetric response is to induce a phase shift (Fig. 3) in the oscillation of the beads measured within the laboratory frame (see [30] (Sect. I.C)). This is captured by an ellipse in the configuration space of the dumbbell, spanned by the coordinates $\vec{x}_1$, and $\vec{x}_2$ of the two oscillating beads. As a consequence of this phase difference, the velocity of the beads with respect to the fluid is not time reversible even though the swimmer deforms in a reciprocal fashion.

The phase shift has two consequences. Firstly, it implies that despite having a force-free swimmer, the instantaneous flow-field generated by the swimmer can have a mono-polar component (see [30] Sect. I.D). Nev-